Supplement of Atmos. Chem. Phys., 25, 16363–16386, 2025
https://doi.org/10.5194/acp-25-16363-2025-supplement

Supplement of

Black carbon aerosols in China: spatial-temporal variations and lessons from long-term atmospheric observations

Huang Zheng et al.

Correspondence to: Shaofei Kong (kongshaofei@cug.edu.cn) and Deping Ding (zytddp@vip.sina.com)

Section S1. Reprocessing of ground observations from previous studies and observations.

In this study, data from 2015 and 2017 were collected from different sources, including published papers, observation networks, and publicly accessible websites. For each data source, different processing methods were applied, as described in detail below.

For data collected from EBAS, the light absorption coefficients (b_{abs}) were converted into eBC mass concentrations using the instrument-specific mass absorption cross-section (MAC). The light absorption coefficients from EBAS were obtained from several instruments, including MAAP-5012, CLAP-10, PASS-3, and Aethalometers (AE16, AE31, AE33, and AE42). For MAAP-5012, CLAP-10, and PASS-3, a MAC value of 6.6 $m^2 g^{-1}$ at 637 nm was used, and it was adjusted for other wavelengths as determined by the instruments. For AE16, AE31, and AE42, a MAC value of 16.6 $m^2 g^{-1}$ at 880 nm was used to convert babs at 880 nm into eBC mass concentrations. For AE33, a MAC value of 7.77 $m^2 g^{-1}$ at 880 nm was used.

To calculate station-specific AAE, b_{abs} measured by the Aethalometer (AE42, AE31, and AE33) were used. Specifically, b_{abs} at 370 nm and 880 nm were used to calculate the AAE value (AAE = $\log(b_{abs\_370} / b_{abs\_880}) / \log(880 / 370)$). Similarly, eBC sources were apportioned using the default AAE combination (AAE_{lf} = 1.0 and AAE_{sf} = 2.0) and wavelengths of 370 nm and 880 nm.

For data collected from the US EPA, the annual mean value for "Black carbon at 880 nm" was used and reported as eBC concentrations. Additionally, the “UV carbon at 370 nm” along with "Black carbon at 880 nm" were used to calculate AAE and apportion eBC sources. Specifically, “UV carbon at 370 nm” and "Black carbon at 880 nm" were converted into babs at 370 nm and 880 nm by multiplying by 39.5 $m^2 g^{-1}$ and 16.6 $m^2 g^{-1}$, respectively. The AAE calculation and BC source apportionment were conducted as discussed for EBAS data.

For data collected from UK AIR, the eBC mass concentration at 880 nm and “UVBC” were used. The babs at 370 nm were calculated as 39.5*(BC + UVBC). The methods for calculating AAE and BC source apportionment were as described above. To ensure robust results, a data availability threshold of 50% was applied to data collected from EBAS, US EPA, and UK AIR.

For data collected from published papers, if eBC source apportionment results were reported, the AAE value was derived from these results. A cross-check between this method and the AAE calculated as the ratio of b_{abs} at two wavelengths showed an uncertainty of approximately 5%.

To calculate the trends of BC from different sources, the annual values were used, and the slope was calculated using the Theil-Sen method, consistent with the data processing in this study. For trends reported by previous studies, we only selected papers that used the Theil-Sen method.

Table S1 Details information of black carbon monitoring station in this study.

Code	Site name	Type [a]	Lon	Lat	MAC (m^2 g^{-1}) [b]	Instrument
AK	Akadala	B	87.97	47.10	8.9	AE31
UR	Urumqi	U	87.56	43.85	8.9	AE31
TZ	Tzhong	RU	83.67	39.00	8.9	AE31
HM	Hami	RU	93.52	42.82	8.9	AE31
EJ	Ejilaqi	RU	101.07	41.95	8.9	AE31
DUH	Dunhuang	RU	94.68	40.15	8.9	AE31
WLG	Waliguan	B	100.62	36.27	14	AE31&AE33
ZR	Zhurihe	RU	112.90	42.40	11.2	AE31
YL	Yulin	RU	109.78	38.27	7.3	AE31
YS	Yushe	RU	112.98	37.07	12.3	AE31
LFS	Longfengshan	B	127.60	44.73	14.4	AE31
XL	Xilinhaote	RU	116.12	43.95	11.2	AE31
TL	Tongliao	RU	122.27	43.60	14.4	AE31
CC	Changchun	U	125.22	43.90	14.4	AE31
AS	Anshan	U	123.00	41.08	14.4	AE31
SY	Shenyang	U	123.52	41.73	14.4	AE31
BX	Benxi	U	123.78	41.32	14.4	AE31
FS	Fushun	U	124.08	41.92	14.4	AE31
SDZ	Shangdianzi	B	117.12	40.65	11.2	AE31 &AE33
GXT	Guanxiangtai	U	116.47	39.80	11.2	AE31
DL	Dalian	U	121.63	38.90	14.4	AE31
HUM	Huimin	RU	117.53	37.48	11.2	AE31
LAS	Lasa	U	91.13	29.67	8.8	AE31
CDU	Chengdu	U	103.83	30.70	14.1	AE31
XGL	Shangri−L	B	99.70	27.83	14	AE31&AE33
ZZ	Zhengzhou	U	113.65	34.72	12.3	AE31
XA	Xi'an	U	108.97	34.43	9.4	AE31
XF	Xiangyang	U	112.17	32.03	14	AE31
YC	Yichang	U	111.30	30.70	14	AE31
WH	Wuhan	U	114.13	30.62	10.2	AE31
JS	Jinsha	B	114.20	29.63	12.3	AE31&AE33
GL	Guilin	RU	110.30	25.32	13.4	AE31
SX	Shouxian	RU	116.78	32.55	14	AE31
DT	Dongtan	RU	122.00	31.50	12.3	AE31
PD	Pudong	U	121.55	31.22	14	AE31
LA	Lin'an	B	119.73	30.30	12.3	AE31&AE33
HAZ	Hangzhou	U	120.17	30.23	14	AE31
DH	Dinghai	RU	122.10	30.03	14	AE31
LUS	Lushan	RU	115.98	29.58	12.3	AE31
WZ	Wenzhou	U	120.65	28.03	14	AE31
HJ	Hongjia	U	121.42	28.62	14	AE31

Code	Site name	Type [a]	Lon	Lat	MAC ($m^2\ g^{-1}$) [b]	Instrument
GZ	Guangzhou	U	113.33	23.17	14	AE31
DG	Dongguan	U	113.73	22.97	8.8	AE31
NN	Nanning	U	108.22	22.63	13.4	AE31
PY	Panyu	RU	113.32	22.93	8.8	AE31
SZ	Shenzhen	U	114.00	22.53	8.8	AE31
HZ	Haizhu	U	113.34	23.07	8.8	AE31
LS	Lishui	U	119.92	28.45	14	AE31
GL	Gaolan	RU	103.93	36.35	7.3	AE31
CDE	Changde	RU	111.68	29.05	18	AE31

[a] B: Baseline station; RU: Rural station; U: Urban station.

[b] MAC: mass attenuation cross-section for AE31 and mass absorption cross-section for AE33. The station-specific MAC value at 880 nm (for AE31) is from Guo et al. (2020) except Wuhan, which is from Zheng et al. (2021).

Table S2 Station specific (SS) AAE values derived from frequency distributions and BC source apportionment results (mean ± standard deviation) derived from station specific AAE values and default AAE combination (AAE_{lf} = 1.0 and AAE_{sf} = 2.0) and their changes (defined as the differences between SS AAE and default AAE).

Code	SS AAE		eBC_{lf} (%)			eBC_{sf} (%)		
	AAE_{lf}	AAE_{sf}	SS AAE	Default	Delta	SS AAE	Default	Delta
UR	1.02	1.70	54.2 ± 23.1	70 ± 16.3	−15.8	45.8 ± 23.1	30.0 ± 16.3	15.8
TZ	0.89	2.53	66.5 ± 24.9	49.7 ± 32.4	16.8	33.5 ± 24.9	50.3 ± 32.4	−16.8
HM	1.00	2.22	57.2 ± 26.4	46.5 ± 29.2	10.7	42.8 ± 26.4	53.5 ± 29.2	−10.7
ZR	0.79	2.09	52.5 ± 23.3	53.6 ± 27.5	−1.1	47.5 ± 23.3	46.4 ± 27.5	1.1
YS	0.75	1.68	50.0 ± 24.2	76.4 ± 20.0	−26.4	50.0 ± 24.2	23.6 ± 20.0	26.4
LFS	0.91	1.79	45.6 ± 24.0	61.9 ± 21.6	−16.3	54.4 ± 24	38.1 ± 21.6	16.3
XL	0.91	1.92	57.0 ± 25.5	64.2 ± 25.5	−7.2	43.0 ± 25.5	35.8 ± 25.5	7.2
CC	0.90	1.61	36.4 ± 26.1	65.5 ± 21.8	−29.1	63.6 ± 26.1	34.5 ± 21.8	29.1
AS	0.87	1.89	47.7 ± 28.7	57.9 ± 29.0	−10.2	52.3 ± 28.7	42.1 ± 29.0	10.2
SY	0.90	1.61	44.4 ± 25.6	72.1 ± 18.9	−27.7	55.6 ± 25.6	27.9 ± 18.9	27.7
BX	0.89	1.58	41.2 ± 25.9	72.4 ± 18.2	−31.2	58.8 ± 25.9	27.6 ± 18.2	31.2
FS	0.89	1.63	44.7 ± 22.0	72.1 ± 16.0	−27.4	55.3 ± 22.0	27.9 ± 16.0	27.4
SDZ	0.86	1.74	45.7 ± 27.8	66.6 ± 24.2	−20.9	54.3 ± 27.8	33.4 ± 24.2	20.9
HUM	0.90	1.81	44.5 ± 24.8	59.4 ± 24.1	−14.9	55.5 ± 24.8	40.6 ± 24.1	14.9
LAS	0.91	1.70	54.2 ± 25.5	73.8 ± 20.6	−19.6	45.8 ± 25.5	26.2 ± 20.6	19.6
XGL	0.93	1.88	51.2 ± 32.8	58.9 ± 32.5	−7.7	48.8 ± 32.8	41.1 ± 32.5	7.7
ZZ	0.83	1.54	53.8 ± 23.2	84.1 ± 13.7	−30.3	46.2 ± 23.2	15.9 ± 13.7	30.3
XA	0.87	1.64	52.4 ± 23.1	77.1 ± 17.4	−24.7	47.6 ± 23.1	22.9 ± 17.4	24.7
XF	0.92	1.64	59.2 ± 20.7	80.3 ± 12.9	−21.1	40.8 ± 20.7	19.7 ± 12.9	21.1
WH	0.94	1.60	46.2 ± 28.3	71.1 ± 22.3	−24.9	53.8 ± 28.3	28.9 ± 22.3	24.9
SX	0.96	1.57	58.8 ± 21.0	81.5 ± 11.5	−22.7	41.2 ± 21.0	18.5 ± 11.5	22.7
PD	0.98	1.69	55.4 ± 25.0	71.5 ± 21.3	−16.1	44.6 ± 25.0	28.5 ± 21.3	16.1
LA	0.92	1.56	34.8 ± 24.8	67.1 ± 21.3	−32.3	65.2 ± 24.8	32.9 ± 21.3	32.3
HAZ	0.89	1.45	60.5 ± 21.1	89.5 ± 9.3	−29	39.5 ± 21.1	10.5 ± 9.30	29
DH	0.87	1.51	56.4 ± 22.9	85.8 ± 12.4	−29.4	43.6 ± 22.9	14.2 ± 12.4	29.4
LUS	0.84	1.71	48.9 ± 26.8	70.4 ± 24.8	−21.5	51.1 ± 26.8	29.6 ± 24.8	21.5
HJ	0.94	1.58	60.4 ± 21.8	82.3 ± 14.2	−21.9	39.6 ± 21.8	17.7 ± 14.2	21.9
DG	0.89	1.58	56.1 ± 27.6	79.8 ± 20.8	−23.7	43.9 ± 27.6	20.2 ± 20.8	23.7
NN	0.94	1.56	47.0 ± 20.1	75.7 ± 13.1	−28.7	53.0 ± 20.1	24.3 ± 13.1	28.7
PY	0.98	1.52	52.5 ± 17.3	80.0 ± 8.50	−27.5	47.5 ± 17.3	20.0 ± 8.50	27.5
SZ	0.88	1.43	52.3 ± 20.2	87.1 ± 10.7	−34.8	47.7 ± 20.2	12.9 ± 10.7	34.8
HZ	0.93	1.51	62.7 ± 20.5	87.1 ± 9.70	−24.4	37.3 ± 20.5	12.9 ± 9.70	24.4
LS	0.89	1.53	52.6 ± 22.2	82.1 ± 12.2	−29.5	47.4 ± 22.2	17.9 ± 12.2	29.5
GL	1.00	1.74	55.5 ± 22.1	69.8 ± 16.2	−14.3	44.5 ± 22.1	30.2 ± 16.2	14.3

Table S3 Relative uncertainty of the Aethalometer model in each station using the propagation of errors

Code	eBC_{sf}	eBC_{lf}	Code	eBC_{sf}	eBC_{lf}
UR	32.0%	35.3%	XA	30.7%	24.4%
TZ	53.8%	25.6%	XF	30.8%	27.5%
HM	41.8%	47.2%	WH	30.4%	35.6%
ZR	32.6%	33.0%	SX	37.7%	34.3%
YS	25.0%	27.4%	PD	35.2%	27.2%
LFS	19.8%	40.8%	LA	27.6%	54.0%
XL	29.0%	23.7%	HAZ	53.8%	33.8%
CC	21.6%	51.8%	DH	37.3%	34.7%
AS	24.3%	30.0%	LUS	23.9%	25.4%
SY	24.8%	36.5%	HJ	39.8%	29.6%
BX	25.3%	47.4%	DG	35.4%	27.3%
FS	22.7%	37.0%	NN	30.4%	45.8%
SDZ	20.7%	29.4%	PY	44.3%	45.4%
HUM	21.6%	32.6%	SZ	49.1%	48.6%
LAS	24.2%	27.8%	HZ	52.7%	31.1%
XGL	28.6%	23.9%	LS	33.2%	39.9%
ZZ	33.2%	33.5%	GL	30.5%	30.8%

Table S4 Hyperparameter tunning results for RF model used to normalize the influence of weather on black carbon and its source.

Code	min.node.size			mtry			num.trees		
	eBC	eBC_{lf}	eBC_{sf}	eBC	eBC_{lf}	eBC_{sf}	eBC	eBC_{lf}	eBC_{sf}
HM	1	4	3	11	7	9	754	694	457
DUH	6	3	1	13	9	11	436	536	348
ZR	1	1	1	7	7	6	980	980	495
YS	4	1	4	7	6	9	903	505	921
LFS	4	3	4	9	9	9	549	536	549
XL	8	2	10	5	4	8	483	428	123
CC	1	2	5	12	12	8	480	813	359
AS	3	1	1	6	6	10	500	139	760
SY	4	5	2	7	7	8	195	468	235
BX	4	6	4	9	9	9	415	149	415
FS	1	2	2	10	7	7	687	432	621
SDZ	1	4	2	5	4	7	146	573	621
GXT	1	6	1	11	10	12	675	822	751
DL	4	4	4	9	9	7	921	921	903
HUM	1	2	1	10	11	7	825	408	133
CDU	2	1	2	12	10	11	533	610	817
XGL	2	3	2	13	13	13	437	244	437
ZZ	4	2	4	10	8	9	852	208	905
XA	4	1	5	10	11	12	606	675	585
LA	1	2	2	7	8	8	980	814	814
LUS	4	5	2	13	9	5	585	235	375
NN	2	2	2	6	6	6	773	773	773
PY	4	5	6	9	6	8	549	848	370
SZ	2	4	1	7	6	11	374	777	887
GL	7	1	5	8	11	9	694	826	311

Table S5 The surface BC concentrations derived from different CMIP6 historical simulations and other models.

Model name	Institution, country	Ensembles	Resolution	Experiment	Variables
CESM2-WACCM	NCAR, USA	1	100 km	Historical	mmrbc
CNRM-ESM2-1	CNRM-CERFACS, France	2	250 km	Historical	mmrbc
GFDL-ESM4	NOAA-GFDL, USA	1	100 km	Historical	mmrbc
GISS-E2-1-G-CC	NASA-GISS/USA	5	250 km	Historical	mmrbc
MRI-ESM2-0	MRI/Japan	6	100 km	Historical	mmrbc
UKESM1-0-LL	NIWA, MOHC, NIMS-KMA	3	250 km	Historical	mmrbc
MERRA2	NOAA, USA	—	$0.625^{\circ} \times 0.5^{\circ}$	−	BCSMASS
TAP	Tsinghua, China	—	10 km	−	BC

Table S6 Statistics (mean ± standard deviation, 5th, and 95th percentiles) of black carbon concentrations (eBC), BC from liquid fuel (eBC_{lf}) and solid fuel (eBC_{sf}) combustion, and AAE values in each station.

Code	eBC (μg m^{-3})		eBC_{lf} (μg m^{-3})		eBC_{sf} (μg m^{-3})		AAE_{370_950}	
	Mean ± SD	[5th, 95th]	Mean ± SD	[5th, 95th]	Mean ± SD	[5th, 95th]	Mean ± SD	[5th, 95th]
UR	1.69 ± 1.53	[0.31, 4.81]	0.89 ± 0.81	[0.03, 2.42]	0.80 ± 0.95	[0.09, 2.83]	1.37 ± 0.20	[1.11, 1.70]
TZ	0.80 ± 0.89	[0.18, 2.08]	0.55 ± 0.66	[0.00, 1.52]	0.25 ± 0.40	[0.03, 0.76]	1.60 ± 0.45	[1.04, 2.38]
HM	2.09 ± 2.57	[0.27, 7.39]	1.03 ± 1.34	[0.00, 3.57]	1.07 ± 1.72	[0.04, 4.67]	1.66 ± 0.40	[1.09, 2.37]
ZR	0.50 ± 0.56	[0.10, 1.41]	0.26 ± 0.32	[0.00, 0.79]	0.23 ± 0.34	[0.03, 0.75]	1.56 ± 0.35	[1.04, 2.16]
YS	2.07 ± 1.35	[0.49, 4.59]	1.12 ± 0.98	[0.03, 2.89]	0.96 ± 0.76	[0.20, 2.47]	1.27 ± 0.27	[0.91, 1.70]
LFS	0.67 ± 0.75	[0.11, 1.98]	0.27 ± 0.35	[0.00, 0.84]	0.39 ± 0.52	[0.03, 1.25]	1.53 ± 0.30	[1.04, 2.04]
XL	0.11 ± 0.12	[0.02, 0.30]	0.07 ± 0.08	[0.00, 0.21]	0.04 ± 0.06	[0.00, 0.12]	1.41 ± 0.32	[0.98, 1.95]
CC	2.63 ± 2.76	[0.39, 7.78]	1.00 ± 1.54	[0.00, 3.63]	1.62 ± 1.70	[0.15, 4.91]	1.45 ± 0.29	[1.01, 1.96]
AS	1.36 ± 1.10	[0.36, 3.40]	0.71 ± 0.71	[0.00, 2.03]	0.66 ± 0.64	[0.08, 1.95]	1.55 ± 0.43	[0.93, 2.31]
SY	6.67 ± 6.52	[0.73, 20.4]	3.12 ± 3.65	[0.00, 10.3]	3.54 ± 3.88	[0.34, 12.0]	1.36 ± 0.26	[1.00, 1.79]
BX	4.95 ± 4.31	[0.76, 13.8]	2.01 ± 2.25	[0.00, 6.51]	2.94 ± 2.90	[0.27, 8.81]	1.37 ± 0.23	[1.02, 1.75]
FS	2.22 ± 1.87	[0.43, 5.88]	0.99 ± 0.97	[0.01, 2.81]	1.23 ± 1.18	[0.17, 3.49]	1.38 ± 0.21	[1.04, 1.72]
SDZ	1.30 ± 1.30	[0.15, 3.96]	0.63 ± 0.77	[0.00, 2.03]	0.68 ± 0.85	[0.08, 2.46]	1.38 ± 0.31	[0.96, 1.86]
HUM	1.31 ± 1.35	[0.26, 3.95]	0.61 ± 0.69	[0.00, 1.89]	0.70 ± 0.82	[0.10, 2.29]	1.46 ± 0.29	[1.06, 1.90]
LAS	2.24 ± 2.74	[0.42, 6.88]	1.20 ± 1.41	[0.00, 3.76]	1.04 ± 1.82	[0.14, 3.64]	1.31 ± 0.26	[1.01, 1.77]
XGL	0.16 ± 0.12	[0.03, 0.40]	0.10 ± 0.11	[0.00, 0.31]	0.06 ± 0.06	[0.00, 0.17]	1.38 ± 0.37	[0.94, 2.10]
ZZ	4.58 ± 5.39	[0.56, 15.5]	2.50 ± 3.49	[0.13, 8.82]	2.08 ± 2.74	[0.17, 7.45]	1.19 ± 0.20	[0.91, 1.51]
XA	4.75 ± 7.19	[0.25, 20.7]	2.96 ± 4.87	[0.01, 13.26]	1.78 ± 2.80	[0.14, 8.13]	1.29 ± 0.21	[1.01, 1.67]
XF	1.90 ± 1.40	[0.37, 4.78]	1.13 ± 0.93	[0.13, 3.06]	0.76 ± 0.70	[0.08, 2.13]	1.27 ± 0.18	[1.01, 1.57]
WH	5.26 ± 4.42	[0.97, 14.2]	2.73 ± 3.21	[0.00, 9.09]	2.53 ± 2.27	[0.27, 7.07]	1.25 ± 0.21	[0.98, 1.62]
SX	1.52 ± 1.16	[0.38, 3.87]	0.87 ± 0.75	[0.14, 2.34]	0.65 ± 0.69	[0.08, 1.96]	1.26 ± 0.18	[1.02, 1.57]
PD	1.31 ± 1.04	[0.32, 3.37]	0.82 ± 0.80	[0.00, 2.35]	0.49 ± 0.36	[0.09, 1.21]	1.31 ± 0.24	[1.04, 1.68]
LA	1.79 ± 1.15	[0.49, 4.02]	0.71 ± 0.79	[0.00, 2.17]	1.08 ± 0.67	[0.24, 2.38]	1.30 ± 0.16	[1.07, 1.57]
HAZ	1.71 ± 1.18	[0.45, 4.07]	1.11 ± 1.01	[0.13, 3.06]	0.60 ± 0.43	[0.11, 1.48]	1.11 ± 0.13	[0.93, 1.36]
DH	0.82 ± 0.65	[0.16, 2.11]	0.47 ± 0.43	[0.04, 1.33]	0.35 ± 0.35	[0.04, 1.06]	1.19 ± 0.18	[0.94, 1.51]
LUS	0.60 ± 0.51	[0.07, 1.56]	0.33 ± 0.36	[0.00, 1.00]	0.27 ± 0.24	[0.03, 0.73]	1.30 ± 0.28	[0.94, 1.76]

Code	eBC (μg m^{-3})		eBC_{lf} (μg m^{-3})		eBC_{sf} (μg m^{-3})		AAE_{370_950}	
	Mean ± SD	[5^{th}, 95^{th}]	Mean ± SD	[5^{th}, 95^{th}]	Mean ± SD	[5^{th}, 95^{th}]	Mean ± SD	[5^{th}, 95^{th}]
HJ	1.56 ± 1.11	[0.38, 3.77]	0.98 ± 0.79	[0.09, 2.53]	0.58 ± 0.52	[0.07, 1.58]	1.24 ± 0.18	[1.01, 1.52]
DG	2.08 ± 1.55	[0.50, 5.03]	1.30 ± 1.25	[0.00, 3.64]	0.78 ± 0.62	[0.02, 1.99]	1.19 ± 0.23	[0.89, 1.59]
NN	1.51 ± 1.32	[0.35, 4.10]	0.68 ± 0.70	[0.06, 1.91]	0.83 ± 0.84	[0.14, 2.65]	1.28 ± 0.17	[1.07, 1.53]
PY	2.71 ± 1.87	[0.83, 6.25]	1.43 ± 1.13	[0.24, 3.52]	1.27 ± 1.01	[0.29, 3.21]	1.22 ± 0.11	[1.09, 1.41]
SZ	2.07 ± 1.45	[0.51, 4.84]	1.10 ± 0.94	[0.11, 2.85]	0.97 ± 0.78	[0.16, 2.45]	1.14 ± 0.14	[0.95, 1.35]
HZ	3.38 ± 2.62	[0.95, 8.13]	2.26 ± 2.10	[0.28, 6.11]	1.11 ± 0.88	[0.25, 2.87]	1.17 ± 0.13	[1.00, 1.42]
LS	1.11 ± 0.94	[0.26, 2.49]	0.56 ± 0.51	[0.06, 1.31]	0.55 ± 0.62	[0.06, 1.51]	1.23 ± 0.17	[0.96, 1.50]
GL	1.39 ± 1.09	[0.29, 3.55]	0.77 ± 0.71	[0.08, 2.14]	0.62 ± 0.60	[0.08, 1.85]	1.41 ± 0.21	[1.12, 1.74]

Table S7 Trends of black carbon and its sources during the study period using the Theil−Sen method.

Code	eBC		eBC_{lf}		eBC_{sf}		Period
	µg m^{-3} yr^{-1}	% yr^{-1}	µg m^{-3} yr^{-1}	% yr^{-1}	µg m^{-3} yr^{-1}	% yr^{-1}	
HM	−0.18 [−0.35, −0.17] ***	−4.94 [−7.44, −4.82] ***	−0.08 [−0.13, −0.05] **	−4.55 [−6.49, −2.90] **	−0.12 [−0.21, −0.09] ***	−5.77 [−7.90, −4.92] ***	2008−2020
DUH	−0.07 [−0.40, +0.22]	−1.91 [−6.24, +7.12]	−0.03 [−0.19, +0.11]	−1.79 [−5.59, +6.66]	−0.05 [−0.27, +0.19]	−2.11 [−8.67, +11.7]	2008−2017
ZR	−0.08 [−0.17, −0.01] *	−8.04 [−12.0, −2.23] *	−0.05 [−0.09, −0.01] **	−8.80 [−11.7, −2.96] **	−0.03 [−0.06, +0.00] *	−7.07 [−10.7, −1.34] *	2008−2020
YS	+0.04 [−0.19, +0.27]	+3.13 [−7.46, +100]	+0.01 [−0.10, +0.17]	+1.92 [−6.74, −125]	+0.03 [−0.09, +0.11]	+6.34 [−7.21, +158]	2008−2019
LFS	−0.13 [−0.21, −0.06] **	−6.56 [−8.64, −3.65] **	−0.05 [−0.08, −0.03] **	−6.55 [−8.98, −4.55] **	−0.08 [−0.12, −0.04] **	−6.95 [−8.18, −3.47] **	2008−2017
XL	−0.07 [−0.13, −0.03] *	−7.85 [−11.8, −5.81] *	−0.04 [−0.08, −0.01] *	−7.65 [−11.2, −2.42] *	−0.02 [−0.04, −0.02] *	−7.7 [−11.16, −6.23] *	2008−2017
CC	−0.08 [−0.37, +0.86]	−2.30 [−6.55, +86.9]	−0.06 [−0.20, +0.34]	−3.30 [−7.43, +38.7]	−0.01 [−0.19, +0.39]	−0.74 [−6.52, +80.4]	2008−2018
AS	−0.17 [−0.21, −0.11] ***	−5.49 [−6.44, −4.93] ***	−0.11 [−0.15, −0.08] ***	−6.05 [−7.03, −6.02] ***	−0.04 [−0.07, −0.03] **	−4.11 [−6.11, −2.95] **	2008−2020
SY	+0.16 [−0.16, +0.52]	+5.31 [−4.23, +42.0]	+0.06 [−0.15, +0.26]	+3.17 [−6.88, +24.5]	+0.09 [−0.02, +0.32]	+6.95 [−0.99, +89.9]	2008−2019
BX	+0.06 [−0.20, +0.33]	+1.75 [−5.39, +18.4]	−0.08 [−0.20, +0.17]	−3.79 [−9.14, +18.2]	+0.13 [+0.02, +0.22] *	+12.1 [+1.73, +34.0] *	2008−2019
FS	−0.11 [−0.25, +0.21]	−3.62 [−6.20, +9.40]	−0.11 [−0.19, +0.01]	−5.96 [−8.12, +0.60]	−0.01 [−0.09, +0.09]	−0.49 [−5.05, +8.67]	2008−2018
SDZ	−0.11 [−0.15, −0.03] *	−5.12 [−5.92, −1.37] *	−0.06 [−0.08, −0.04] ***	−5.12 [−5.92, −3.30] ***	−0.04 [−0.08, +0.03]	−4.39 [−6.05, +3.44]	2009−2020
GXT	−0.03 [−0.50, +0.43]	−0.55 [−8.85, +17.7]	+0.00 [−0.40, +0.42]	+0.00 [−9.91, +131]	+0.00 [−0.12, +0.10]	−0.20 [−6.03, +7.91]	2008−2019
DL	−0.05 [−0.09, +0.22]	−2.94 [−4.66, +26.8]	+0.00 [−0.03, +0.21]	+0.01 [−3.95, −127]	−0.04 [−0.08, +0.01]	−4.27 [−5.70, +1.65]	2008−2020
HUM	−0.56 [−1.25, +0.01]	−13.1 [−19.0, +0.69]	−0.32 [−0.73, +0.00]	−13.1 [−18.8, +0.19]	−0.22 [−0.64, +0.05]	−11.8 [−13.9, +17.9]	2008−2017
CDU	−0.51 [−0.81, +0.04]	−6.40 [−8.28, +0.64]	−0.44 [−0.58, −0.13] *	−8.39 [−9.56, −3.00] *	−0.10 [−0.27, +0.24]	−3.76 [−6.79, +13.5]	2010−2020
XGL	+0.00 [−0.01, +0.01]	−0.10 [−4.21, +9.37]	+0.00 [−0.01, +0.00]	−1.72 [−4.65, +7.99]	+0.00 [+0.00, +0.01]	+4.11 [−3.86, +26.6]	2009−2020
ZZ	−0.54 [−1.15, −0.07] *	−6.41 [−10.8, −1.12] *	−0.29 [−0.77, +0.03]	−6.69 [−11.4, +1.14]	−0.25 [−0.38, −0.07] *	−7.18 [−8.87, −2.73] *	2009−2019
XA	−0.50 [−0.86, +0.07]	−5.57 [−7.63, +1.13]	−0.38 [−0.70, +0.09]	−6.26 [−9.69, +1.99]	−0.18 [−0.29, −0.08] *	−5.73 [−8.30, −3.25] *	2008−2020
LA	−0.19 [−0.22, −0.15] **	−6.74 [−7.53, −5.81] **	−0.11 [−0.15, −0.07] **	−8.74 [−9.33, −6.51] **	−0.08 [−0.12, −0.01] *	−5.03 [−6.94, −0.52] *	2011−2020
LUS	−0.10 [−0.16, −0.07] ***	−6.34 [−8.53, −4.52] ***	−0.06 [−0.10, −0.03] **	−6.48 [−9.07, −3.93] **	−0.04 [−0.07, −0.02] ***	−7.19 [−9.39, −4.36] ***	2008−2019
NN	−0.17 [−0.24, −0.14] ***	−5.50 [−6.77, −4.79] ***	−0.09 [−0.13, −0.07] ***	−5.54 [−6.66, −4.70] ***	−0.07 [−0.10, −0.06] ***	−5.22 [−6.18, −4.65] ***	2008−2020
PY	−0.53 [−0.74, −0.19] *	−7.80 [−9.74, −3.54] *	−0.40 [−0.52, −0.09] *	−9.25 [−9.67, −2.88] *	−0.13 [−0.30, −0.03] *	−5.40 [−8.49, −1.45] *	2008−2016
SZ	−0.25 [−0.28, −0.23] ***	−8.71 [−9.67, −8.65] ***	−0.13 [−0.16, −0.08] **	−8.52 [−8.63, −5.88] **	−0.12 [−0.17, −0.08] ***	−9.32 [−11.6, −7.85] ***	2013−2020
GL	−0.12 [−0.19, −0.06] ***	−5.56 [−7.95, −3.59] ***	−0.05 [−0.10, −0.02] **	−4.75 [−6.94, −1.64] **	−0.05 [−0.08, −0.02] ***	−5.83 [−7.53, −3.56] ***	2008−2020

*, **, and *** represent the trends that are significant at 0.05, 0.01, and 0.001 levels.

Table S8 Reported eBC mass concentrations, eBC_{sf} fraction, and AAE values from different observation networks and published papers.

Country	Site/code	Type	Lon	Lat	Alt (m)	Period	eBC	eBC_{sf}	AAE	Instrument	Matrix	Sources
India	Srinagar	U	74.83	34.13	1591	2017	4.3	0.22	1.31	AE31	PM_{10}	
India	Gulmarg	M	74.4	34.05	2703	2017	2.4	0.17	1.24	AE42-HS	PM_{10}	(Romshoo et al., 2023)
India	New Delhi	U	77.19	28.55	210	2017	12.3	0.26	1.35	AE33	PM_{10}	
Ireland	Carnsore Point		−6.35	52.17	0.217	2016−2017	0.32			AE33	PM_{10}	(Spohn et al., 2022)
India	Ranichauri		78.04	30.3	2200	2016	1.93			AE33	NP	(Pandey et al., 2020)
India	Chirbasa		79.08	30.98	3600	2016	0.395			AE33	NP	(Negi et al., 2019)
India	Ranichauri	B	78.08	30.25		2016−2018	1.74	0.34	1.42	AE33	$PM_{2.5}$	
India	Srinagar	V	78.08	34.08		2016−2018	11.7	0.23	1.30	AE33	$PM_{2.5}$	
India	Chandigarh	U	76.88	30.73		2016−2018	11.2	0.16	1.21	AE33	$PM_{2.5}$	
India	Varasi	U	83.01	25.3		2016−2018	8.68	0.27	1.34	AE33	$PM_{2.5}$	
India	Jodhpur	D	73.01	26.3		2016−2018	4.51	0.18	1.24	AE33	$PM_{2.5}$	
India	New Delhi	U	77.2	28.58		2016−2018	13.6	0.18	1.24	AE33	$PM_{2.5}$	
India	Ranchi	U	85.31	23.31		2016−2018	4.42	0.23	1.30	AE33	$PM_{2.5}$	
India	Kolkata	C	88.45	22.65		2016−2018	12.1	0.12	1.16	AE33	$PM_{2.5}$	(Kumar et al., 2020)
India	Guwahati	U	91.58	26.1		2016−2018	6.65	0.17	1.23	AE33	$PM_{2.5}$	
India	Bhuj	D	69.66	23.25		2016−2018	2.02	0.22	1.29	AE33	$PM_{2.5}$	
India	Pune	U	73.85	18.53		2016−2018	6.96	0.12	1.16	AE33	$PM_{2.5}$	
India	gpur	U	79.05	21.1		2016−2018	4.48	0.21	1.27	AE33	$PM_{2.5}$	
India	Visakhapatm	C	83.23	17.71		2016−2018	6.05	0.09	1.12	AE33	$PM_{2.5}$	
India	Thiruvananthapuram	C	76.95	8.48		2016−2018	4.65	0.19	1.25	AE33	$PM_{2.5}$	
India	Port Blair	BA	92.71	11.66		2016−2018	2.51	0.1	1.14	AE33	$PM_{2.5}$	
India	Vijayawada	SUB	80.62	16.44	30	2016	3.44	0.21	1.66	AE33		(Prasad et al., 2018)
India	Ahmednagar		74.74	19.09	649	2016	12.9	0.08	1.1	AE33	$PM_{2.5}$	(Kolhe et al., 2019)
India	Pashan		73.8	18.53	559	2016	6.07	0.13	1.17	AE33	$PM_{2.5}$	
Australia	Beresfield		151.67	−32.80	16	2015	1.27	0.15	1.20	AE33		(Duc et al., 2020)
Australia	Newcastle		151.76	−32.93	19	2015	0.97	0.17	1.23	AE33		
Czech	OK	RB	15.08	49.58	534	2015−2017	0.68	0.31	1.41	AE31	PM_{10}	(Mbengue et al., 2020)

Country	Site/code	Type	Lon	Lat	Alt (m)	Period	eBC	eBC_{sf}	AAE	Instrument	Matrix	Sources
Polar	Syowa	P	39.35	−69.00	29	2015−2017	0.0034			AE31		(Hara et al., 2019)
Spain	Barcelo	U	2.12	41.39	80	2015−2017	1.49	0.08	1.17	AE33	PM_{10}	(Savadkoohi et al., 2023)
Switzerland	Bern-Bollwerk	TRA	7.44	46.95	536	2015−2017	1.09	0.28	1.20	AE33	$PM_{2.5}$	
Romania	Bucharest	SUB	26.03	44.35	70	2016, 2017	2.07	0.34	1.44	AE33	PM_{10}	
Spain	Grada	U	−3.58	37.18	680	2015, 2016	2.62	0.19	1.28	AE33	Aerosol	
Sweden	Hornsgatan	U	18.05	59.32	669	2015−2017	1.09	0.11	1.15	AE33	PM_{10}	
Spain	Madrid	SUB	−3.73	40.46	162	2015−2017	1.70	0.13	1.19	AE33	$PM_1/PM_{2.5}$	
France	Paris	U	2.16	48.71	25	2015−2017	0.76	0.23	1.38	AE33	$PM_{2.5}$	
Sweden	Torkel	U	18.06	59.32	48	2015−2017	0.33	0.23	1.32	AE33	PM_1	
Switzerland	Zurich	UB	8.53	47.38	409	2015−2017	1.01	0.23	1.31	AE33	$PM_{2.5}$	
UK	UKA00451	RB	−3.24	55.79	260	2015−2017	0.15	0.29	1.29	AE22	$PM_{2.5}$	UK AIR
UK	UKA00503	UB	−6.25	54.86	59	2015−2017	0.91	0.40	1.48	AE22	$PM_{2.5}$	
UK	UKA00212	UB	−5.93	54.60	10	2015−2017	1.09	0.19	1.26	AE22	$PM_{2.5}$	
UK	UKA00655	UB	−1.83	52.51	134	2015−2017	1.14	0.13	1.19	AE22	$PM_{2.5}$	
UK	UKA00626	TRA	−1.83	52.51	93	2015−2017	2.11	0.08	1.12	AE22	$PM_{2.5}$	
UK	UKA00217	UB	−3.18	51.48	12	2015−2017	0.88	0.19	1.25	AE22	$PM_{2.5}$	
UK	UKA00614	RB	−1.44	51.15	78	2015−2017	0.39	0.37	1.44	AE22	$PM_{2.5}$	
UK	UKA00481	RB	0.58	51.31	182	2015−2017	0.47	0.26	1.33	AE22	$PM_{2.5}$	
UK	UKA00602	TRA	−4.24	55.86	35	2015−2017	1.51	0.10	1.14	AE22	$PM_{2.5}$	
UK	UKA00576	UB	−4.24	55.87	40	2015−2017	0.84	0.10	1.13	AE22	$PM_{2.5}$	
UK	UKA00570	UB	−6.01	54.54	35	2015−2017	0.71	0.31	1.40	AE22	$PM_{2.5}$	
UK	UKA00315	TRA	−0.15	51.52	35	2015−2017	4.67	0.06	1.09	AE22	$PM_{2.5}$	
UK	UKA00253	UB	−0.21	51.52	5	2015−2017	1.01	0.19	1.25	AE22	$PM_{2.5}$	
UK	UKA00393	SUBB	−7.45	54.82	28	2015−2017	1.22	0.48	1.57	AE22	$PM_{2.5}$	
USA	2916	SUB	−71.36	41.84	15	2015−2017	0.41			AE16	$PM_{2.5}$	US EPA
USA	48101	SUB	−83.21	42.23	181	2015−2017	0.57			AE21	$PM_{2.5}$	

Country	Site/code	Type	Lon	Lat	Alt (m)	Period	eBC	eBC_{sf}	AAE	Instrument	Matrix	Sources
USA	7002	U	−74.13	40.67	3	2015−2017	1.20			AE33	$PM_{2.5}$	
USA	94710	U	−122.30	37.86	2.7	2015−2017	1.14			AE33	$PM_{2.5}$	
USA	63107	U	−90.20	38.66	150	2015−2017	0.82	0.32	1.41	AE33	$PM_{2.5}$	
USA	64133	SUB	−94.45	39.05	293	2015−2017	0.86	0.23	1.32	AE33	$PM_{2.5}$	
USA	84010	SUB	−111.88	40.90	1309	2015−2017	0.64			AE21	$PM_{2.5}$	
USA	8103	U	−75.13	39.93	4	2015−2017	0.75			AE33	$PM_{2.5}$	
USA	2905	U	−71.41	41.81	9	2015−2017	0.37			AE16	$PM_{2.5}$	
USA	45225	U	−84.54	39.15	162	2015−2017	2.10			AE33	$PM_{2.5}$	
USA	6513	U	−72.90	41.30	3.6	2015−2017	0.67	0.23	1.32	AE33	$PM_{2.5}$	
USA	2119	U	−71.08	42.33	6	2015−2017	0.72			AE33	$PM_{2.5}$	
USA	48223	U	−83.27	42.39	0.5	2015−2017	0.61	0.46	1.56	AE33	$PM_{2.5}$	
USA	7202	SUB	−74.21	40.64	5	2015−2017	1.58			AE33	$PM_{2.5}$	
USA	48223	SUB	−83.27	42.39	0.5	2015−2017	1.06	0.26	1.35	AE33	$PM_{2.5}$	
USA	46517	RU	−85.97	41.66	197	2015−2017	0.44	0.57	1.67	AE22ER	$PM_{2.5}$	
USA	47710	SUB	−87.58	38.01	116	2015−2017	0.48	0.64	1.73	AE22ER	$PM_{2.5}$	
USA	94933	SUB	−122.69	38.02	75	2015−2017	0.82			AE33	$PM_{2.5}$	US EPA
USA	63110	U	−90.28	38.63	310	2015−2017	0.93	0.25	1.34	AE33	$PM_{2.5}$	
USA	7024	U	−73.97	40.85	87	2015−2017	0.82			AE33	$PM_{2.5}$	
USA	46403	SUB	−87.30	41.61	122	2015−2017	0.69	0.22	1.31	AE21ER	$PM_{2.5}$	
USA	1301	U	−72.60	42.61	267	2015−2017	0.46			AE33	$PM_{2.5}$	
USA	6120	U	−72.68	41.77	8	2015−2017	0.90	0.29	1.39	AE33	$PM_{2.5}$	
USA	80204	SUB	−105.02	39.73	1583	2015−2017	1.84	0.09	1.14	AE33	$PM_{2.5}$	
USA	46218	U	−86.11	39.81	230	2015−2017	0.62	0.37	1.48	AE21ER	$PM_{2.5}$	
USA	46201	U	−86.13	39.79	195	2015−2017	1.20	0.25	1.34	AE33	$PM_{2.5}$	
USA	10455	U	−73.90	40.82	17	2015−2017	0.88			AE21ER	$PM_{2.5}$	
USA	94607	U	−122.26	37.79	3.9	2015−2017	1.27			AE33	$PM_{2.5}$	
USA	1104	U	−72.59	42.11	31	2015−2017	0.87			AE33	$PM_{2.5}$	
USA	94551	U	−121.78	37.69	137	2015−2017	0.65			AE33	$PM_{2.5}$	
USA	48152	SUB	−83.43	42.42	0.1	2015−2017	0.61	0.43	1.54	AE33	$PM_{2.5}$	
USA	6108	U	−72.63	41.78	15	2015−2017	0.48	0.34	1.44	AE33	$PM_{2.5}$	
USA	20001	SUB	−77.01	38.92	50	2015−2017	0.63		1.47	AE21	$PM_{2.5}$	

Country	Site/code	Type	Lon	Lat	Alt (m)	Period	eBC	eBC_{sf}	AAE	Instrument	Matrix	Sources
USA	27616	U	−78.57	35.86	100	2015−2017	0.44	0.09	1.14	AE21ER	$PM_{2.5}$	
USA	19801	RU	−75.56	39.74	0	2015−2017	0.65			AE33	$PM_{2.5}$	
USA	6759	SUB	−73.30	41.82	505	2015−2017	0.20	0.36	1.46	AE33	$PM_{2.5}$	
USA	33607	U	−82.47	27.96	6	2015−2017	0.92			AE33	$PM_{2.5}$	
USA	2908	U	−71.42	41.83	23	2015−2017	1.64			Multiple	$PM_{2.5}$	
USA	55404	U	−93.25	44.97	259	2015−2017	0.87	0.23	1.32	AE33	$PM_{2.5}$	
USA	2109	SUB	−71.05	42.36	7	2015−2017	0.90			Multiple	$PM_{2.5}$	
USA	30034	U	−84.27	33.70	238	2015−2017	1.86			MAAP	$PM_{2.5}$	
USA	30313	U	−84.39	33.78	286	2015−2017	2.22			MAAP	$PM_{2.5}$	
USA	94607	SUB	−122.28	37.81	0	2015−2017	0.70			AE33	$PM_{2.5}$	
USA	15221	SUB	−79.86	40.44	355	2015−2017	0.99	0.17	1.24	AE33	$PM_{2.5}$	
USA	48120	U	−83.15	42.31	0	2015−2017	0.78			AE21	$PM_{2.5}$	
USA	14610	RU	−77.55	43.15	137	2015−2017	0.35			AE21ER	$PM_{2.5}$	
USA	28138	U	−80.40	35.55	240	2015−2017	0.44	0.26	1.36	AE22ER	$PM_{2.5}$	US EPA
USA	95814	SUB	−121.50	38.59	12.8	2015−2017	1.20			AE33	$PM_{2.5}$	
USA	95821	U	−121.37	38.61	8	2015−2017	0.63			AE33	$PM_{2.5}$	
USA	95122	SUB	−121.85	37.34	30.9	2015−2017	1.00			AE33	$PM_{2.5}$	
USA	33702	U	−82.67	27.83	15	2015−2017	0.64			AE33	$PM_{2.5}$	
USA	98104	U	−122.32	47.60	15	2015−2017	1.49	0.19	1.27	AE33	$PM_{2.5}$	
USA	98144	U	−122.33	47.60	26	2015−2017	1.05	0.31	1.41	AE33	$PM_{2.5}$	
USA	98144	SUB	−122.31	47.60	58	2015−2017	0.80	0.29	1.38	AE33	$PM_{2.5}$	
USA	33782	SUB	−82.71	27.85	4.41	2015−2017	0.40			AE33	$PM_{2.5}$	
USA	30034	SUB	−84.29	33.69	308	2015−2017	1.19			AE21	$PM_{2.5}$	
USA	97224	SUB	−122.75	45.39	53	2015−2017	1.13	0.34	1.44	Multiple	$PM_{2.5}$	
USA	2125	U	−71.06	42.33	15	2015−2017	1.21			AE33	$PM_{2.5}$	
USA	6810	SUB	−73.44	41.40	116	2015−2017	0.66	0.36	1.47	AE33	$PM_{2.5}$	
Australia	AU0002G	C	144.69	−40.68	94	2015−2017	0.04			MAAP	PM_1	
Bulgaria	BG0001R	NP	23.58	42.17	2971	2015−2017	0.18			CLAP-10	Aerosol	
Bolivia	BO0001R	NP	−68.10	−16.20	5320	2015−2017	0.07	0.16	1.02	AE31	PM10	EBAS
Cada	CA0011R	RU	−79.78	44.23	255	2015−2017	0.26			CLAP-10	PM_1	
Cada	CA0420G	P	−62.34	82.50	210	2015−2017	0.01	0.09	0.93	AE31	Aerosol	

Country	Site/code	Type	Lon	Lat	Alt (m)	Period	eBC	eBC_{sf}	AAE	Instrument	Matrix	Sources
Switzerland	CH0001G	M	7.99	46.55	3578	2015−2017	0.02	0.12	1.09	AE33	Aerosol	
Switzerland	CH0002R	RU	6.94	46.81	489	2015−2017	0.68	0.24	1.33	AE33	$PM_{2.5}$	
Switzerland	CH0005R	NP	8.46	47.07	1031	2015−2017	0.25	0.22	1.36	AE33	$PM_{2.5}$	
Chile	CL0001R	M	−70.80	−30.17	2220	2015−2017	0.04	0.18	1.14	AE31	Aerosol	
Cyprus	CY0002R	RU	33.06	35.04	520	2015−2017	0.11	0.06	0.95	AE31	Aerosol	
Czech	CZ0003R	RU	15.08	49.57	535	2015−2017	0.16	0.18	1.15	AE31	PM_{10}	
Germany	DE0002R	NP	10.76	52.80	74	2015−2017	0.54			MAAP	PM_{10}	
Germany	DE0003R	NP	7.91	47.91	1205	2015−2017	0.42			MAAP	PM_{10}	
Germany	DE0003R	NP	7.91	47.91	1205	2015−2017	0.42			MAAP	PM_1	
Germany	DE0007R	NP	13.03	53.17	62	2015−2017	0.43			MAAP	PM_{10}	
Germany	DE0043G	M	11.01	47.80	975	2015−2017	0.35			MAAP	PM_{10}	
Germany	DE0044R	RU	12.93	51.53	86	2015−2017	0.65			MAAP	PM_{10}	
Germany	DE0054R	M	10.98	47.42	2671	2015−2017	0.10			MAAP	PM_{10}	
Germany	DE0055B	NP	12.43	51.35	113	2015−2017	0.93			MAAP	PM_{10}	
Germany	DE0060G	P	−8.27	−70.67	42	2015−2017	0.00			MAAP	Aerosol	
Germany	DE0066K	NP	12.41	51.35	120	2015−2017	1.58			MAAP	PM_1	EBAS
Germany	DE0066K	NP	12.41	51.35	120	2015−2017	1.58			MAAP	PM_{10}	
Germany	DE0067K	NP	12.38	51.34	111	2015−2017	2.15			MAAP	PM_{10}	
Germany	DE0068B	NP	12.30	51.32	122	2015−2017	0.46			MAAP	PM_{10}	
Denmark	DK0025G	P	−38.48	72.58	3238	2015−2017	0.01			CLAP-10	$PM_{2.5}$	
Spain	ES0018G	M	−16.50	28.31	2373	2015−2017	0.16			MAAP	PM_{10}	
Spain	ES0020U	NP	−3.61	37.16	680	2015−2017	2.35			MAAP	PM_{10}	
Spain	ES0022R	M	0.73	42.05	1571	2015−2017	0.20			MAAP	PM_{10}	
Spain	ES0100R	RU	−6.73	37.10	41	2015−2017	0.42			CLAP-10	PM_1	
Spain	ES1778R	NP	2.35	41.77	700	2015−2017	0.36			MAAP	PM_{10}	
Spain	ES1778R	NP	2.35	41.77	700	2015−2017	0.36			MAAP	Aerosol	
Finland	FI0050R	RU	24.28	61.85	181	2015−2017	0.05	0.08	0.93	AE31	PM_{10}	
Finland	FI0096G	RU	24.12	67.97	565	2015−2017	0.02	0.11	0.92	AE31	Aerosol	
France	FR0019R	NP	0.14	42.94	2877	2015−2017	0.01			AE16	PM_{10}	
France	FR0019R	NP	0.14	42.94	2877	2015−2017	0.01			AE16	Aerosol	
France	FR0022R	RU	5.51	48.56	392	2015−2017	0.09	0.13	1.16	AE31	Aerosol	

Country	Site/code	Type	Lon	Lat	Alt (m)	Period	eBC	eBC_{sf}	AAE	Instrument	Matrix	Sources
France	FR0026R	M	55.38	−21.08	2160	2015−2017	0.07	0.15	1.15	AE42	PM_{10}	
France	FR0030R	M	2.96	45.77	1465	2015−2017	0.19			MAAP	Aerosol	
Greece	GR0100B	U	23.82	37.99	270	2015−2017	0.36	0.69	1.16	AE33	PM_{10}	
Greece	GR0101R	M	22.20	37.98	2340	2015−2017	0.03			AE31	PM_{10}	
Hungary	HU0002R	RU	19.58	46.97	125	2015−2017	1.20			CLAP-10	PM_{10}	
Ireland	ID1013R	M	100.32	−0.20	845	2015−2017	0.22	0.16	1.22	AE31	Aerosol	
Italy	IT0009R	M	10.70	44.19	2165	2015−2017	0.22			MAAP	Aerosol	
R. Koera	KR0100R	C	126.33	36.54	46	2015−2017	0.28	0.12	1.10	AE31	PM_{10}	
Netherlands	NL0011R	NP	4.93	51.97	1	2015−2017	0.43			MAAP	PM_{10}	
Norway	NO0002R	RU	8.25	58.39	219	2015−2017	0.63			PSAP-1W	PM_{10}	
Norway	NO0002R	RU	8.25	58.39	219	2015−2017	0.63			PSAP-3W	PM_{10}	
Norway	NO0042G	P	11.89	78.91	474	2015−2017	0.01	0.04	0.36	AE31	PM_{10}	EBAS
Norway	NO0059G	P	2.54	−72.01	1553	2015−2017	0.01			PSAP-3W	PM_{10}	
Puerto Rico	PR0100C	NP	−65.62	18.38	65	2015−2017	0.09			CLAP−10	PM_1	
Russia	RU0100R	C	128.92	71.59	8	2015−2017	0.10			MAAP	PM_{10}	
Chi	TW0100R	NP	120.87	23.47	2862	2015−2017	0.51			PSAP-3W	PM_1	
USA	US0035R	NP	−88.37	40.05	213	2015−2017	0.29			CLAP-10	PM_1	
USA	US3446C	NP	−81.70	36.20	1100	2015−2017	0.26			PSAP-3W	PM_1	
USA	US3446C	NP	−81.70	36.20	1100	2015−2017	0.26			CLAP-10	PM_1	
USA	US6002C	RU	−97.48	36.61	318	2015−2017	0.26			PSAP-3W	PM_1	
USA	US6005G	C	−124.15	41.05	107	2015−2017	0.07			CLAP-10	PM_1	
USA	US9050R	M	−106.74	40.45	3220	2015−2017	0.08			CLAP-10	PM_1	
Vietm	VN0001R	M	103.52	21.57	1466	2015−2017	0.34	0.46	1.46	AE31	Aerosol	

B: Background; BA: Bay; C: Coastal; D: Desert; M: Mountain; NP: Not provided; P: Polar; RB: Rural background; RU: Rural; SUB: Suburban; SUBB: Suburban background; TRA: Traffic; U: Urban; UB: Urban background; V: Valley

Table S9 The detailed information about the station with the continuous measurements of BC from 2008 to 2020 in this study and previous studies or observation networks.

Site name/code	Country	Type [a]	Lon	Lat	Period	Instrument	Slope (% yr^{-1})	Sources
Zabrze	Poland	UB	18.20	50.10	2010−2020	MAAP	−1.46	(Chilinski et al., 2016)
RB2	Finland	RB	24.28	61.85	2008−2018	MAAP&AE31	−6.54	(Luoma et al., 2021)
St. Louis	USA	U	−90.20	38.66	2008−2015	AE21 &AE33	+4.40	US EPA
Providence-Warwick, RI-MA	USA	U	−71.41	41.81	2008−2020	AE16	−3.57	
Boston	USA	U	−71.08	42.33	2008−2020	AE21ER & AE33	−2.22	
Elkhart	USA	RU	−85.97	41.66	2012−2020	AE22	−1.33	
Evansville	USA	SUB	−87.58	38.01	2009−2020	AE22	−1.91	
Lagunitas	USA	SUB	−122.69	38.02	2013−2020	AE22 & AE33	−4.46	
East Providence	USA	SUB	−71.36	41.84	2008−2020	AE16 &AE33	−2.47	
Gary	USA	SUB	−87.30	41.61	2008−2020	AE21	−4.04	
Indiapolis	USA	U	−86.11	39.81	2008−2020	AE21	−3.06	
New York	USA	U	−73.90	40.82	2008−2018	AE21	−4.51	
Springfield	USA	U	−72.59	42.11	2008−2018	AE22 & AE33	−1.08	
Livermore	USA	U	−121.78	37.69	2012−2020	AE16 &AE33	−2.70	
Washington	USA	SUB	−77.01	38.92	2008−2020	AE22 & AE33	−3.41	
Wilmington	USA	RU	−75.56	39.74	2008−2019	AE22 & AE33	−3.89	
Oakland	USA	SUB	−122.28	37.81	2009−2020	AE22 & AE33	−3.07	
Rochester	USA	RU	−77.55	43.15	2008−2018	AE21	−4.72	
Arden−Arcade	USA	U	−121.37	38.61	2008−2020	Multiple	−2.34	
South DeKalb	USA	SUB	−84.29	33.69	2008−2016	AE21ER	−2.63	
DDN	Germany	R	13.74	51.07	2009−2018	MAAP	−11.30	(Sun et al., 2020)
LEI	Germany	R	12.41	51.35	2009−2018	MAAP	−5.00	
LMI	Germany	R	12.38	51.34	2010−2018	MAAP	−5.50	
LTR	Germany	UB	12.43	51.35	2009−2018	MAAP	−4.10	
ANA	Germany	UB	13.00	50.57	2012−2018	MAAP	−6.90	
AUG	Germany	UB	10.91	48.36	2009−2018	Aethalometer	−2.30	
DDW	Germany	UB	13.73	51.04	2012−2018	MAAP	−8.10	
BOS	Germany	UB	7.94	53.00	2009−2014	MAAP	−4.90	
MEL	Germany	RB	12.93	51.53	2009−2018	MAAP	−4.40	
WAL	Germany	RB	10.76	52.80	2009−2018	MAAP	−3.20	
NEU	Germany	RB	13.03	53.14	2010−2018	MAAP	−7.80	
HPB	Germany	M	11.01	47.80	2009−2018	MAAP	−2.80	

Site name/code	Country	Type [a]	Lon	Lat	Period	Instrument	Slope (% yr^{-1})	Sources
SCH	Germany	M	7.91	47.91	2009−2018	MAAP	−1.70	(Sun et al., 2020)
ZSF	Germany	M	10.98	47.42	2009−2018	MAAP	−4.00	
BCN	Spain	UB	2.12	41.39	2012−2020	AE33	−5.37	(Savadkoohi et al., 2023)
GRA	Spain	UB	−3.58	37.18	2012−2020	MAAP&AE33	−2.41	
LND	UK	UB	−0.21	51.52	2012−2020	AE22 & AE33	−8.32	
LEJ	Germany	UB	12.43	51.35	2012−2020	MAAP	−3.60	
NLD	Netherlands	UB	4.49	51.89	2012−2020	MAAP	−4.79	
ZUR	Switzerland	UB	8.53	47.38	2012−2020	AE33	−10.0	
LND	UK	TRA	−0.15	51.52	2012−2020	AE22 & AE33	−10.5	
LEJ	Germany	TRA	12.41	51.35	2012−2020	MAAP	−3.30	
NLD	Netherlands	TRA	4.48	51.89	2012−2020	MAAP	−6.06	
NLD	Netherlands	TRA	4.48	51.91	2012−2020	MAAP	−5.42	
PAR	France	SUB	2.16	48.71	2012−2020	AE33	−5.92	
IPR	Italy	RB	8.63	45.80	2012−2020	MAAP	−3.28	
SMR	Finland	RB	24.30	61.85	2012−2020	AE31 & AE33 & MAAP	−6.36	
Bern-Bollwerk	Switzerland	TRA	7.44	46.95	2013−2018	AE31&AE33	−11.3	(Grange et al., 2020)
Zirich-K aserne	Switzerland	TRA	8.53	47.38	2009−2018	AE31&AE33	−6.36	
Payerne	Switzerland	RU	6.94	46.81	2008−2018	AE31&AE33	+3.00	
Magadino-Cadezzo	Switzerland	RU	8.93	46.16	2008−2018	AE31&AE33	−1.58	
San Vittore	Switzerland	RU	9.11	46.24	2013−2018	AE33	−2.64	
Rigi-Seebodelp	Switzerland	M	8.46	47.07	2013−2018	AE33	−10.8	
Auchencorth Moss	UK	RB	−3.24	55.79	2012−2020	AE22	−6.08	UK AIR
Ballymena Ballykeel	UK	UB	−6.25	54.86	2013−2020	AE22	−7.19	
Belfast Centre	UK	UB	−5.93	54.60	2009−2020	AE22	−5.38	
Birmingham Tyburn	UK	UB	−1.83	52.51	2009−2017	AE22	−3.73	
Detling	UK	RB	0.58	51.31	2012−2020	AE22	−3.95	
Glasgow Townhead	UK	UB	−4.24	55.87	2013−2020	AE22	−5.03	
Kilmakee Leisure Centre	UK	UB	−6.01	54.54	2012−2020	AE22	−5.51	
London Marylebone Road	UK	TR	−0.15	51.52	2009−2020	AE22	−7.83	
London N. Kensington	UK	TR	−0.21	51.52	2009−2020	AE22	−5.68	
Strabane 2	UK	SUBB	−7.45	54.82	2009−2020	AE22	−2.10	

B: baseline; M: Mountain; R: Roadside; RB: Rural background; Ru: Rural; SUB: SUB; SUBB: SUB background; TR: Traffic; U: U; UB: U background

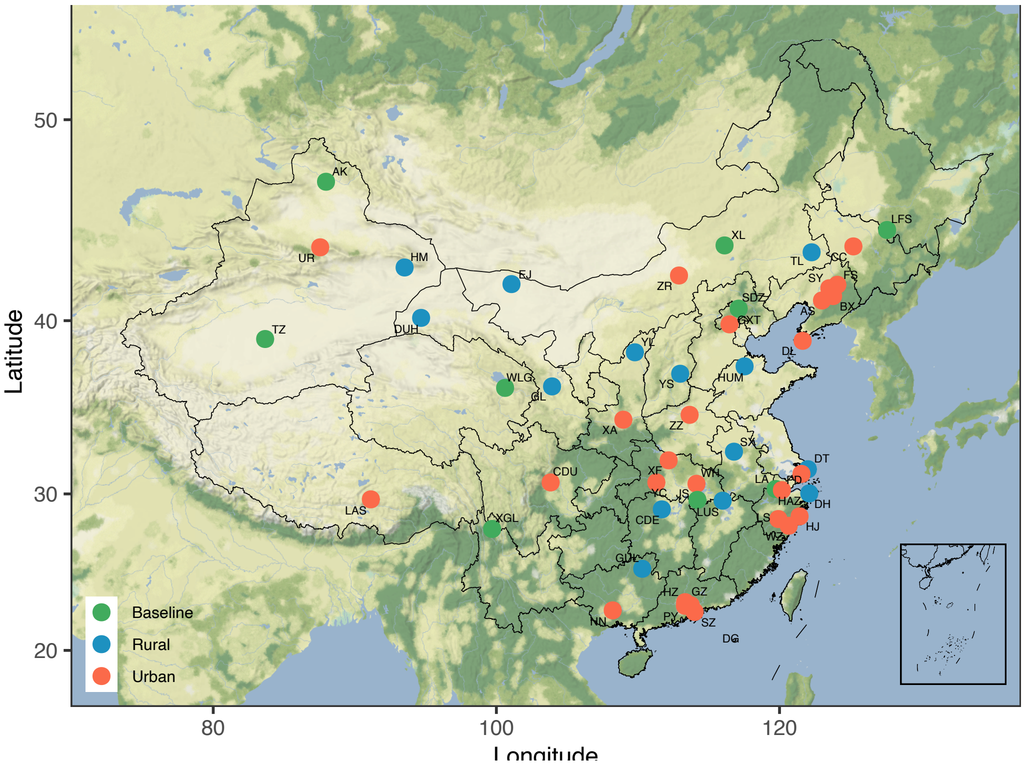

Figure S1 Spatial distribution in BC observational stations in this study.

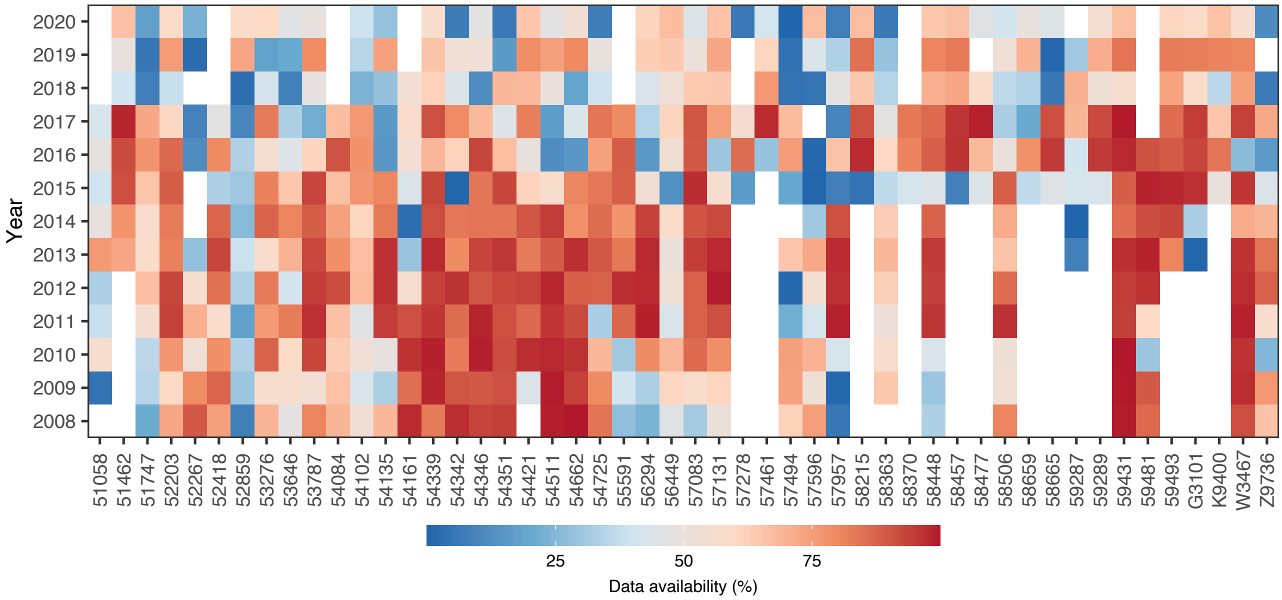

Figure S2 Data availability of black carbon in each station during the observational period from 2008 to 2020.

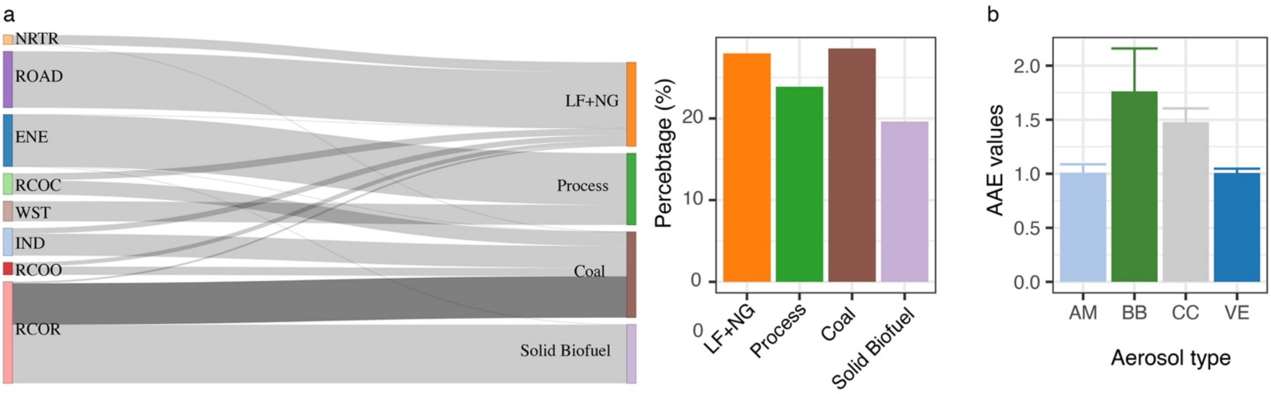

Figure S3 Black carbon from different sectors and fuel types and their percentage to total BC emissions (**a**) and AAE from different types of aerosols including ambient air (AM), biomass burning (BB), coal combustion (CC), and vehicle emissions (VE) from our unpublished data (**b**). The data and more details about the sectors and fuel types can be found in McDuffie et al. (2020).

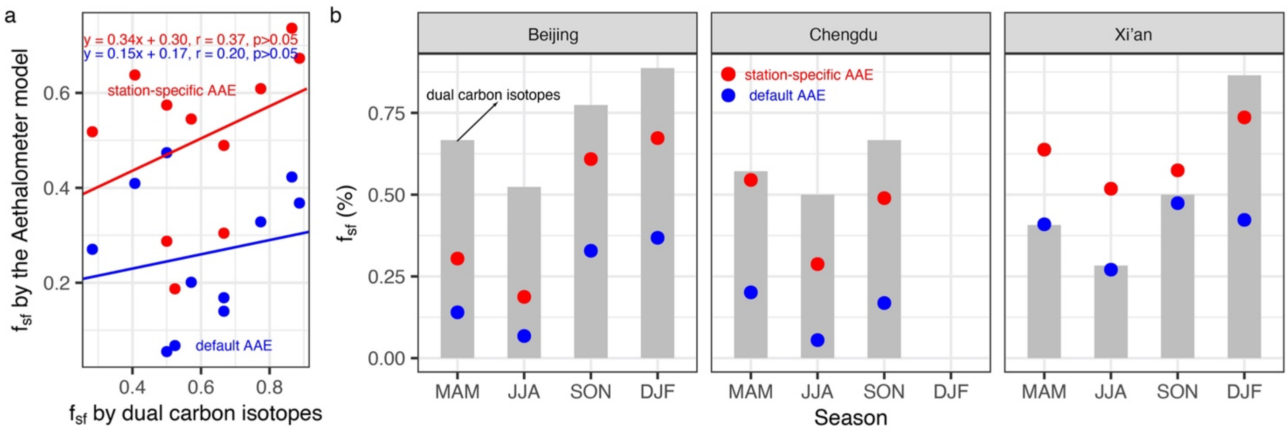

Figure S4 Comparison of BC source apportionment between the Aethalometer model and dual carbon isotopes from previous studies (Fang et al., 2018; Ni et al., 2018). Panel **a** is scatterplot between fraction of BC from solid fuel (f_{sf}) derived from dual carbon isotopes and the Aethalometer model. Panel **b** is the seasonal variations of f_{sf} derived from isotopes (gray bars) and Aethalometer model with default AAE (blue dots) and station-specific AAE (red dots) at three sites.

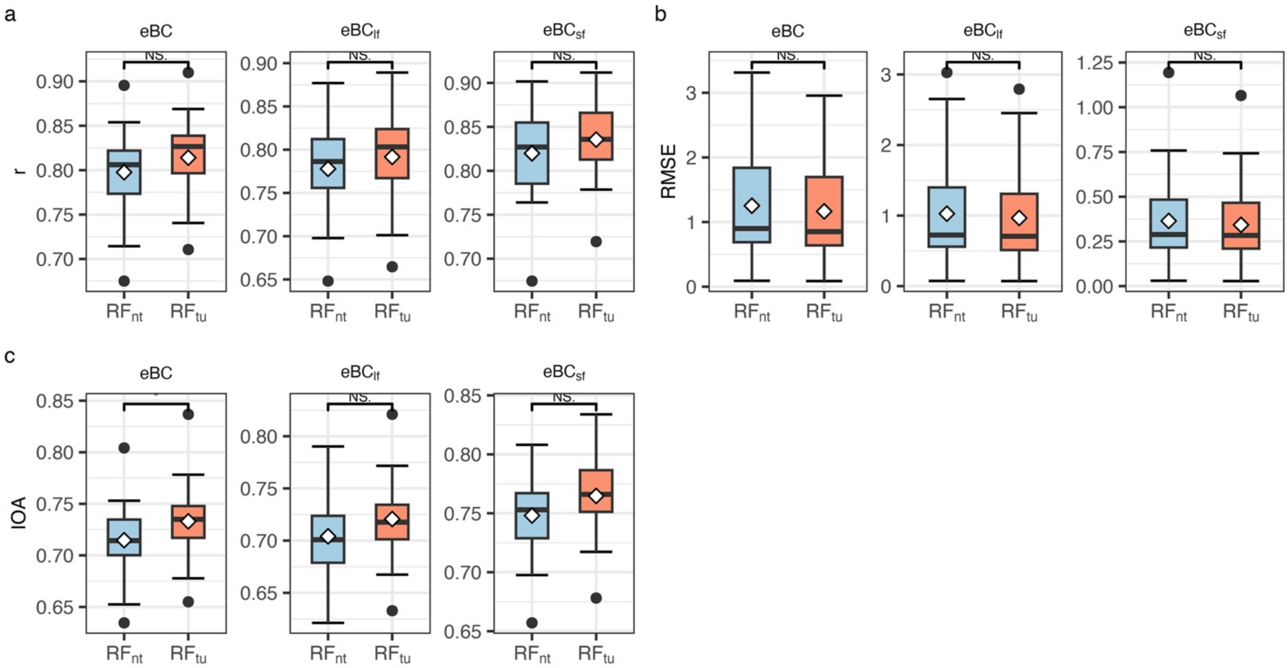

Figure S5 Comparison of model performance evaluation statistics including Pearson correlation coefficient (r, **a**), root mean square error (RMSE, **b**), and index of agreement (IOA, **c**) for eBC, eBC$_{lf}$, and eBC$_{sf}$ by the random forest with parameters not tunned (RF_{nt}) and tuned (RF_{tu}).

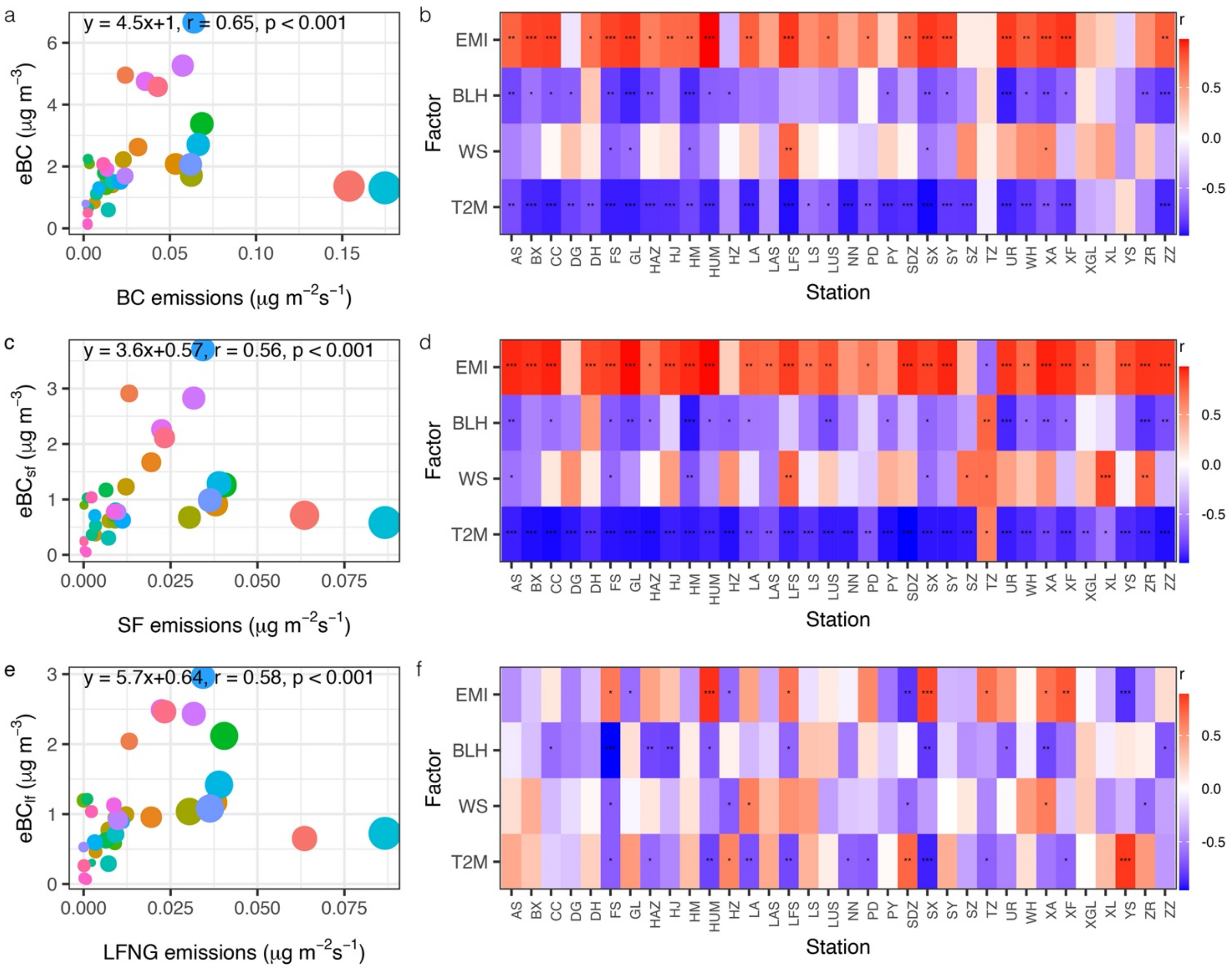

Figure S6 Scatterplots between BC concentrations and emissions from total emissions (**a**), emissions from solid fuel (**c**) and liquid fossil fuel + natural gas (**e**). Panel **b**, **d**, **f** is the correlation between BC concentrations and influencing factors including temperature at 2 m (T2M), wind speed (WS), boundary layer height (BLH), and emissions (EMI). ***, **, * in right panels represent the differences between two group are significant at the 0.001, 0.01, and 0.05 level.

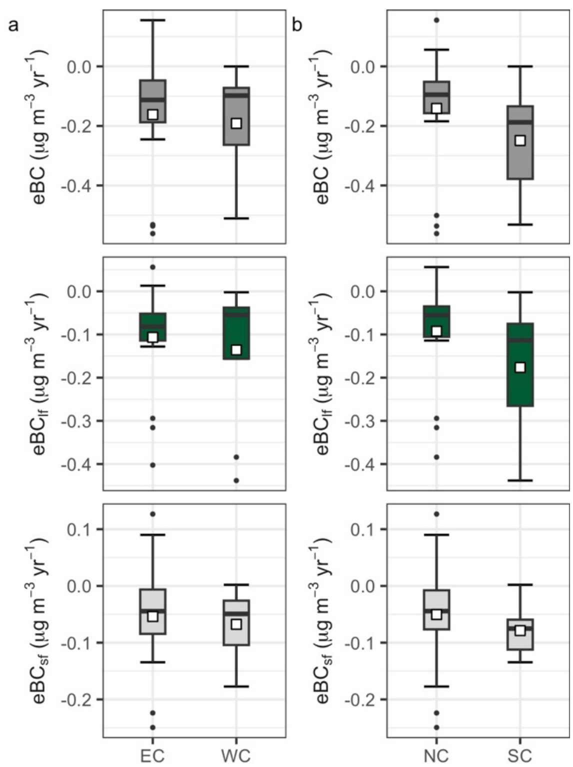

Figure S7 Comparisons of trends of black carbon (eBC) concentration and its sources including liquid fuel (eBC_{lf}) and solid fuel (eBC_{sf}) combustion between eastern China (EC) and western China (WC) in panel **a**, northern China (NC) and southern China (SC) in panel **b**.

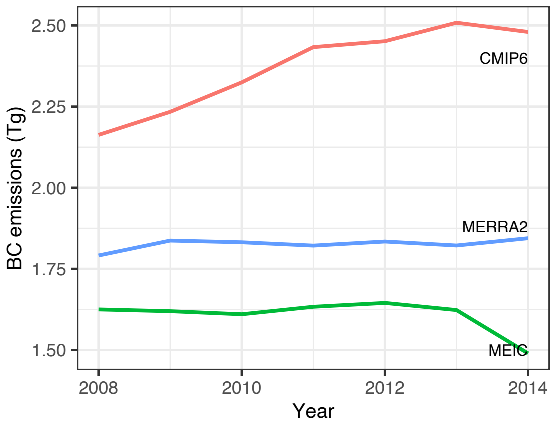

Figure S8 Black carbon emissions in China from different emission inventories from 2008 to 2014.

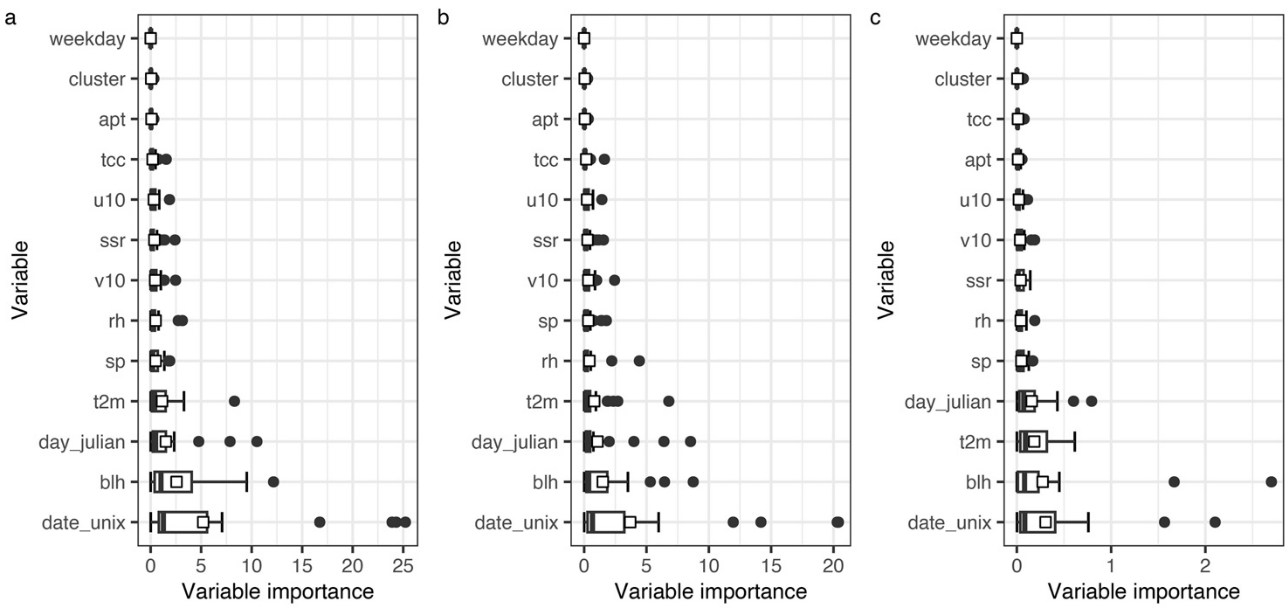

Figure S9 Variable importance for random forest models for eBC (**a**), eBC_{lf} (**b**), and eBC_{sf} (**c**). The boxplot data is from simulation in 25 sites.

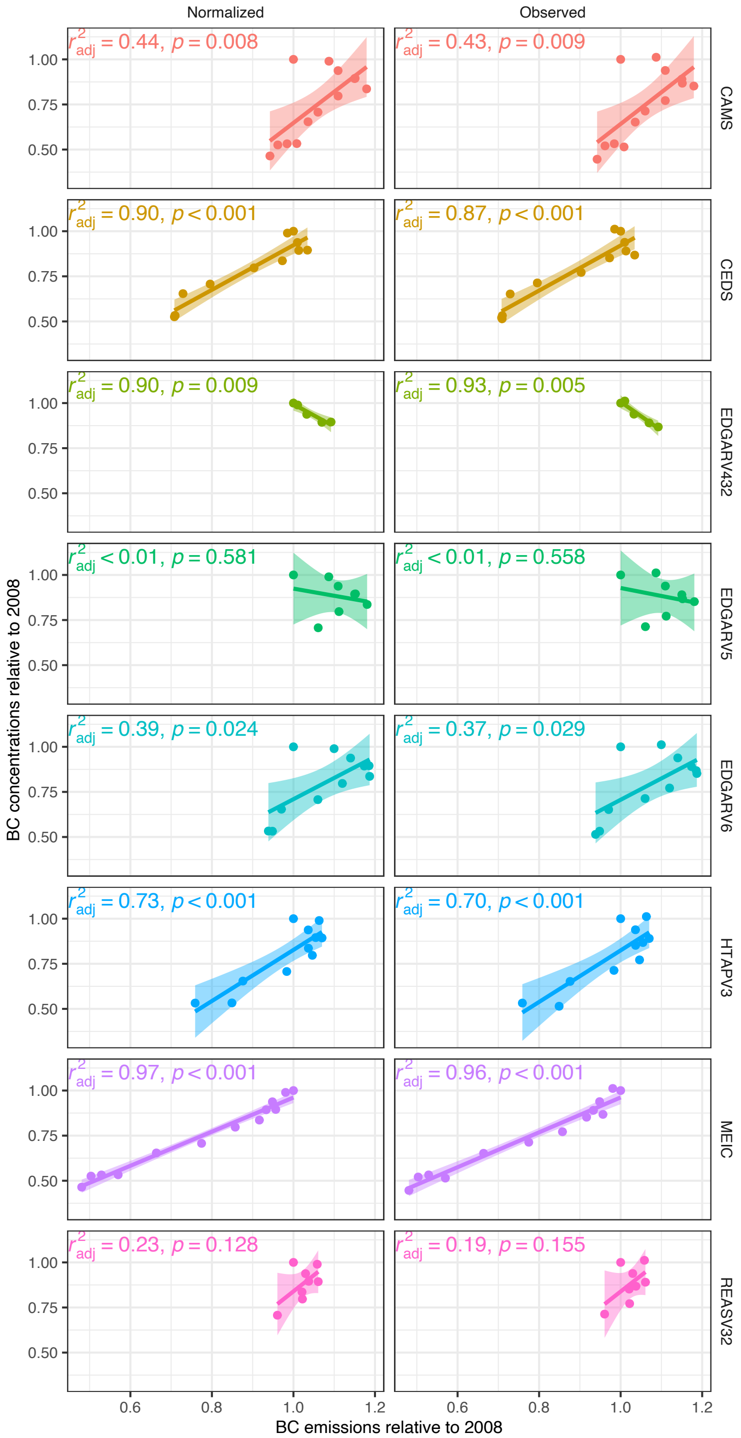

Figure S10 Scatterplot between observed and weather normalized BC concentrations and their emissions from different inventories.

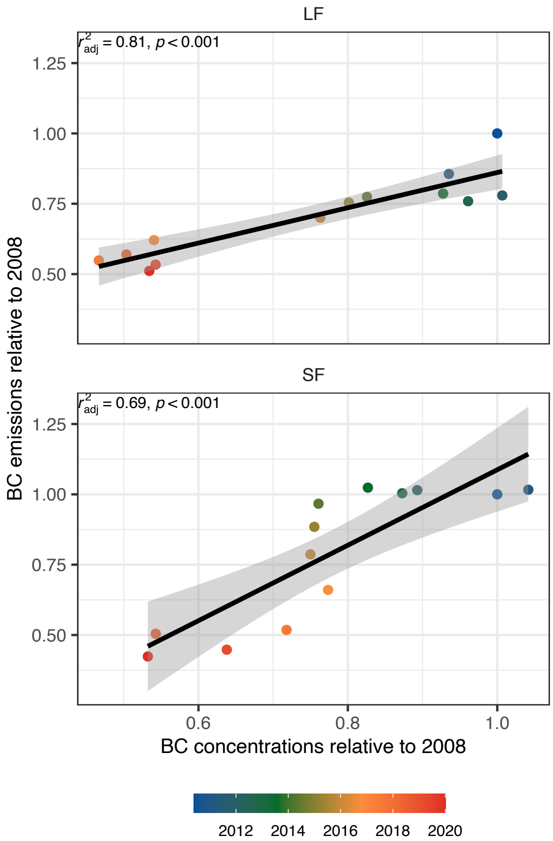

Figure S11 Scatterplot between weather normalized BC source concentrations (including liquid fuel (LF) and solid fuel (SF)) and their emissions derived from MEIC.

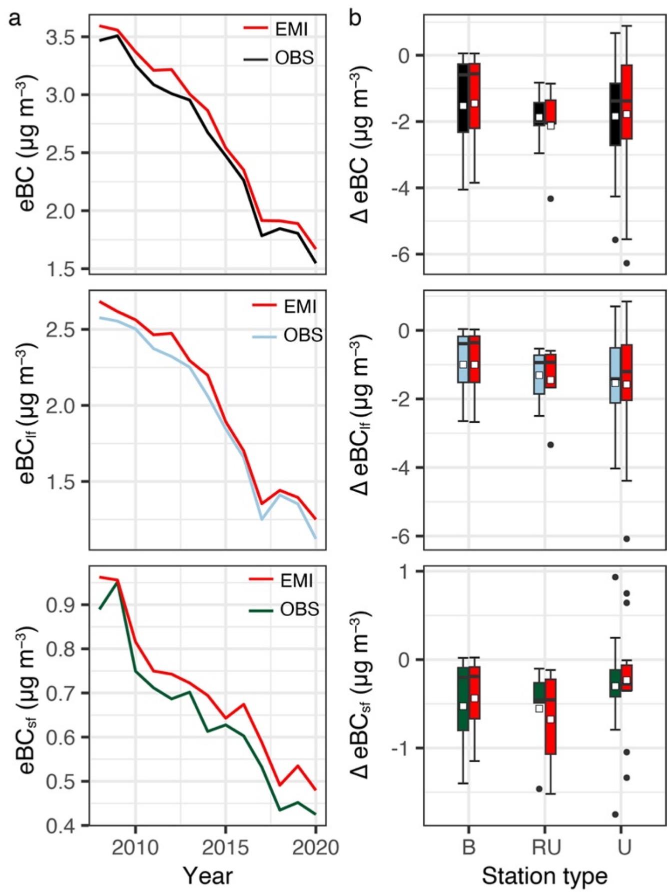

Figure S12 Yearly variations of weather-normalized and observational concentrations of black carbon (**a**) and their changes (expressed as Δ) between 2020 and 2008 (**b**) at different type of stations.

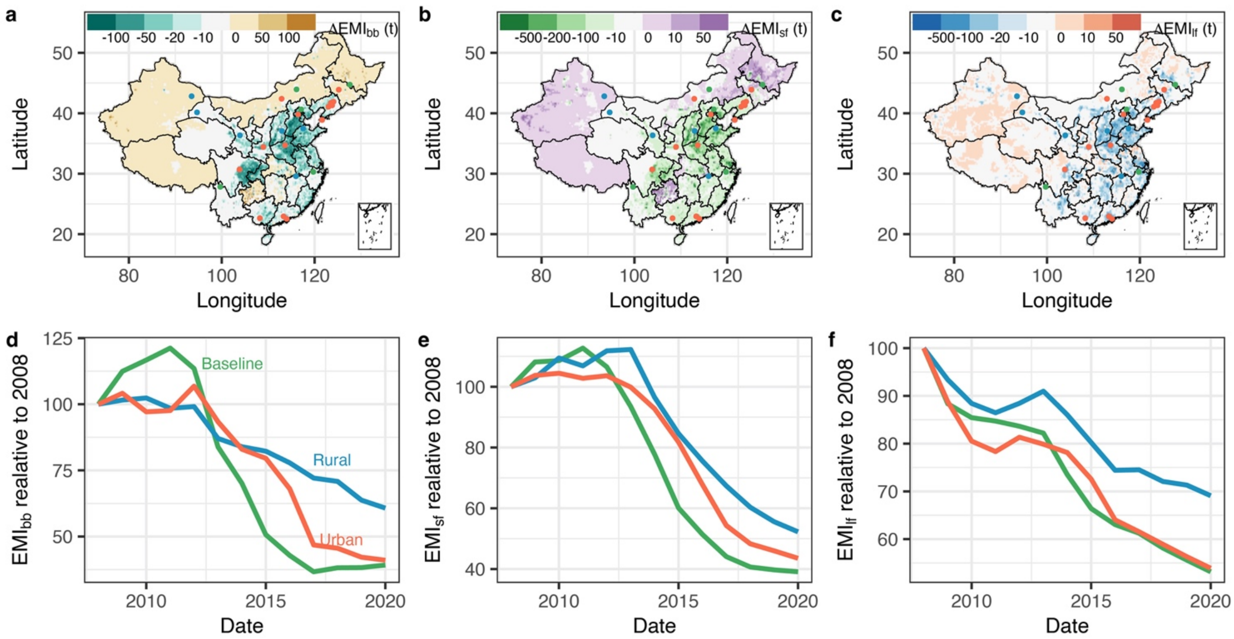

Figure S13 Changes in emission reduction of biomass burning (a), solid fuel combustion (b), and liquid fuel combustion (c) between 2008 and 2020 and their time series of BC emission amount from different fuels compared to 2008 for different station types (d−f).

References

Chilinski, M. T., Markowicz, K. M., and Markowicz, J.: Observation of vertical variability of black carbon concentration in lower troposphere on campaigns in Poland, Atmos. Environ., 137, 155–170, https://doi.org/10.1016/j.atmosenv.2016.04.020, 2016.

Duc, H. N., Shingles, K., White, S., Salter, D., Chang, L. T.-C., Gunashanhar, G., Riley, M., Trieu, T., Dutt, U., Azzi, M., Beyer, K., Hynes, R., and Kirkwood, J.: Spatial-Temporal Pattern of Black Carbon (BC) Emission from Biomass Burning and Anthropogenic Sources in New South Wales and the Greater Metropolitan Region of Sydney, Australia, Atmosphere, 11, 570, https://doi.org/10.3390/atmos11060570, 2020.

Fang, W., Du, K., Andersson, A., Xing, Z., Cho, C., Kim, S., Deng, J., and Gustafsson, Ö.: Dual-isotope constraints on seasonally resolved source fingerprinting of black carbon aerosols in sites of the four emission hot spot regions of China, J. Geophys. Res.: Atmos., 123, https://doi.org/10.1029/2018jd028607, 2018.

Grange, S. K., Lotscher, H., Fischer, A., Emmenegger, L., and Hueglin, C.: Evaluation of equivalent black carbon source apportionment using observations from Switzerland between 2008 and 2018, Atmos. Meas. Tech., 13, 1867–1885, https://doi.org/10.5194/amt-13-1867-2020, 2020.

Hara, K., Sudo, K., Ohnishi, T., Osada, K., Yabuki, M., Shiobara, M., and Yamanouchi, T.: Seasonal features and origins of carbonaceous aerosols at Syowa Station, coastal Antarctica, Atmos. Chem. Phys., 19, 7817–7837, https://doi.org/10.5194/acp-19-7817-2019, 2019.

Kolhe, A. R., Ralegankar, S. D., Safai, P. D., and Aher, G. R.: Absorption properties of black carbon aerosols over environmentally distinct locations in south-western India: Temporal, spectral characterization and source apportionment, J. Atmos. Sol. Terr. Phys., 189, 1–17, https://doi.org/10.1016/j.jastp.2019.03.010, 2019.

Kumar, R. R., Soni, V. K., and Jain, M. K.: Evaluation of spatial and temporal heterogeneity of black carbon aerosol mass concentration over India using three year measurements from IMD BC observation network, Sci. Total Environ., 723, 138060, https://doi.org/10.1016/j.scitotenv.2020.138060, 2020.

Luoma, K., Niemi, J. V., Aurela, M., Fung, P. L., Helin, A., Hussein, T., Kangas, L., Kousa, A., Rönkkö, T., Timonen, H., Virkkula, A., and Petäjä, T.: Spatiotemporal variation and trends in equivalent black carbon in the Helsinki metropolitan area in Finland, Atmos. Chem. Phys., 21, 1173–1189, https://doi.org/10.5194/acp-21-1173-2021, 2021.

McDuffie, E. E., Smith, S. J., O'Rourke, P., Tibrewal, K., Venkataraman, C., Marais, E. A., Zheng, B., Crippa, M., Brauer, M., and Martin, R. V.: A global anthropogenic emission inventory of atmospheric pollutants from sector- and fuel-specific sources (1970–2017): an application of the Community Emissions Data System (CEDS), Earth Syst. Sci. Data, 12, 3413–3442, https://doi.org/10.5194/essd-12-3413-2020, 2020.

Mbengue, S., Serfozo, N., Schwarz, J., Ziková, N., Šmejkalová, A. H., and Holoubek, I.: Characterization of equivalent black carbon at a regional background site in Central Europe: Variability and source apportionment, Environ. Pollut., 260, 113771, https://doi.org/10.1016/j.envpol.2019.113771, 2020.

Negi, P. S., Pandey, C. P., and Singh, N.: Black carbon aerosols in the ambient air of Gangotri Glacier valley of north-western Himalaya in India, Atmos. Environ., 214, 116879, https://doi.org/10.1016/j.atmosenv.2019.116879, 2019.

Ni, H., Huang, R.-J., Cao, J., Liu, W., Zhang, T., Wang, M., Meijer, H. A. J., and Dusek, U.: Source apportionment of carbonaceous aerosols in Xi'an, China: insights from a full year of measurements of radiocarbon and the stable isotope 13C, Atmos. Chem. Phys., 18, 16363–16383, https://doi.org/10.5194/acp-18-16363-2018, 2018.

Pandey, C. P., Singh, J., Soni, V. K., and Singh, N.: Yearlong first measurements of black carbon in the western Indian Himalaya: Influences of meteorology and fire emissions, Atmos. Pollut. Res., 11, 1199–1210, https://doi.org/10.1016/j.apr.2020.04.015, 2020.

Prasad, P., Roja Raman, M., Venkat Ratnam, M., Chen, W.-N., Vijaya Bhaskara Rao, S., Gogoi, M. M., Kompalli, S. K., Sarat Kumar, K., and Suresh Babu, S.: Characterization of atmospheric black carbon over a semi-urban site of Southeast India: Local sources and long-range transport, Atmos. Res., 213, 411–421, https://doi.org/10.1016/j.atmosres.2018.06.024, 2018.

Romshoo, B., Bhat, M. A., and Habib, G.: Black carbon in contrasting environments in India: Temporal variability, source apportionment and radiative forcing, Atmos. Environ., 302, 119734, https://doi.org/10.1016/j.atmosenv.2023.119734, 2023.

Savadkoohi, M., Pandolfi, M., Reche, C., Niemi, J. V., Mooibroek, D., Titos, G., Green, D. C., Tremper, A. H., Hueglin, C., Liakakou, E., Mihalopoulos, N., Stavroulas, I., Artiñano, B., Coz, E., Alados-Arboledas, L., Beddows, D., Riffault, V., De Brito, J. F., Bastian, S., Baudic, A., Colombi, C., Costabile, F., Chazeau, B., Marchand, N., Gómez-Amo, J. L., Estellés, V., Matos, V., Van Der Gaag, E., Gille, G., Luoma, K., Manninen, H. E., Norman, M., Silvergren, S., Petit, J.-E., Putaud, J.-P., Rattigan, O. V., Timonen, H., Tuch, T., Merkel, M., Weinhold, K., Vratolis, S., Vasilescu, J., Favez, O., Harrison, R. M., Laj, P., Wiedensohler, A., Hopke, P. K., Petäjä, T., Alastuey, A., and Querol, X.: The variability of mass concentrations and source apportionment analysis of equivalent black carbon across urban Europe, Environ. Int., 178, 108081, https://doi.org/10.1016/j.envint.2023.108081, 2023.

Spohn, T. K., Martin, D., Geever, M., and O'Dowd, C.: Black carbon measurements from Ireland's Atmospheric Composition and Climate Change (AC3) network, Atmos. Environ., 271, 118932, https://doi.org/10.1016/j.atmosenv.2021.118932, 2022.

Sun, J., Birmili, W., Hermann, M., Tuch, T., Weinhold, K., Merkel, M., Rasch, F., Müller, T., Schladitz, A., Bastian, S., Löschau, G., Cyrys, J., Gu, J., Flentje, H., Briel, B., Asbach, C., Kaminski, H., Ries, L., Sohmer, R., Gerwig, H., Wirtz, K., Meinhardt, F., Schwerin, A., Bath, O., Ma, N., and Wiedensohler, A.: Decreasing trends of particle number and black carbon mass concentrations at 16 observational sites in Germany from 2009 to 2018, Atmos. Chem. Phys., 20, 7049–7068, https://doi.org/10.5194/acp-20-7049-2020, 2020.